Available online at www.sciencedirect.com
SCIENCE DIRECT®
Journal of Catalysis 220 (2003) 92–103
JOURNAL OF CATALYSIS
www.elsevier.com/locate/jcat

m-Xylene transformation over H-MCM-22 zeolite 1. Mechanisms and location of the reactions

S. Laforge,[a] D. Martin,[a] J.L. Paillaud,[b] and M. Guisnet [a,*]

[a] *Laboratoire de Catalyse en Chimie Organique, Université de Poitiers, UMR CNRS 6503, Faculté des Sciences, 40 avenue du Recteur Pineau, 86022 Poitiers cedex, France*

[b] *Laboratoire des Matériaux Minéraux, Université de Haute Alsace, UMR CNRS 7016, Ecole Nationale Supérieure de Chimie de Mulhouse, 3 rue Alfred Werner, 68093 Mulhouse cedex, France*

Received 10 February 2003; revised 20 May 2003; accepted 20 May 2003

Abstract

The transformation of *m*-xylene was investigated at 350 °C over a MWW zeolite sample. The distributions of the desorbed products and of the nondesorbed products ("coke") were established for a large range of contact times, hence of conversions (from 4.8 to 43.7%), and for different times on stream (TOS). A rapid deactivation can be observed during the first 10 min of reaction, followed by a quasi plateau in activity. On the fresh sample (TOS = 2 min), *m*-xylene was transformed into isomers and disproportionation products (toluene and trimethylbenzenes or TMB); TMB underwent various secondary reactions leading to ethyltoluenes, C_2–C_4 alkanes and alkenes, toluene, and coke. Deactivation causes a small decrease in isomerization and suppresses disproportionation and secondary TMB transformations. These latter reactions were demonstrated to occur only in the supercages. On the other hand, approximately 30% of isomerization took place in the supercages and 70%, without any deactivation, in the sinusoidal channels and in the external pockets.

Keywords: MCM-22 zeolite; *m*-Xylene transformation; Reaction scheme; Coke; Formation; Location

1. Introduction

Zeolite MCM-22 (MWW) synthesized by Mobil researchers in 1990 [1] has the particularity to contain two independent noninterconnected pore systems, each accessible through 10-member-ring (MR) apertures [2] and 12-MR pockets on the external surface [3,4]. One of the pore systems consists of two-dimensional sinusoidal channels (4.1 × 5.1 Å); the other comprises large supercages (inner diameter of 7.1 Å defined by 12-MR, height of 18.2 Å), each connected to six others through 10-MR apertures (4.0 × 5.5 Å) [5]; the external pockets correspond to half of supercages (7.1 Å ∅, 7 Å) [3,4].

Many reactions were investigated over protonated samples (H-MCM-22) showing that the behavior of this zeolite was intermediate between those of 12-MR (large pore) and 10-MR (average pore) zeolites [6–14]. First this behavior was related to both the narrow 10-MR apertures of the internal pore systems which give rise to reactant and product shape-selectivity effects and the large supercages which allow bimolecular reactions involving bulky intermediates. However, more recent results demonstrate a significant catalytic action of protonic sites located in the external pockets [3,4,15–18]. In particular, the sites of these pockets were shown to be responsible for the fast, selective, and stable alkylation of benzene with ethene and propene [18–20], which is at the basis of commercial processes.

The transformation of model compounds is well known as an efficient tool for characterizing the acidity [21–23] or the porosity [24–27] of acid catalysts. *m*-Xylene transformation was one of the first proposed for characterizing the pore systems of zeolites [27,28]. Three main reactions can be generally observed: isomerization, disproportionation into toluene and trimethylbenzenes (TMB), and coke formation, with consequently the possibility of various selectivity values, all of them being related to the characteristics of the zeolite pore system: *para*/*ortho*-xylene ratio, toluene/TMB ratio, distributions of TMB, of coke components, disproportionation/isomerization ratio, etc. However, very often, the zeolite pore system is only characterized by

* Corresponding author.
E-mail address: michel.guisnet@univ-poitiers.fr (M. Guisnet).

0021-9517/$ – see front matter
doi:10.1016/S0021-9517(03)00240-9

the *para* to *ortho* and the disproportionation to isomerization ratios which are mainly related to the size of the pore apertures and to that of the cages and channel intersections, respectively.

In this work, a thorough study of *m*-xylene transformation was carried out over a MCM-22 sample. The distribution of the desorbed products and of the nondesorbed ones ("coke") was established at various contact times (hence conversions) and various times on stream. Mechanisms will be proposed for the formation of the various products and the location of the reactions will be discussed.

2. Experimental

2.1. Materials

The MCM-22 sample (total Si/Al ratio of 15) was synthesized at the Laboratoire des Matériaux Minéraux of Mulhouse (France), following the procedure given in Ref. [1]. The as-synthesized MCM-22 sample was calcined in dry air at 550 °C for 12 h, in order to remove the hexamethyleneimine template and to form the supercages from the precursor [3]. Then, it was exchanged twice with a 2 M NH_4NO_3 solution, under stirring at 80 °C for 1 h and calcined at 500 °C for 4 h, under air flow.

2.2. Characterization of fresh and "coked" MCM-22 samples

The porosity of fresh and coked samples was determined by nitrogen sorption at −196 °C carried out with an automatic Micromeritics ASAP 2010 apparatus.

IR spectra were recorded with a Nicolet Magna IR 550 Fourier transform spectrometer. Thin wafers of 5–10 mg/cm^2 were activated in situ in the IR cell under air flow (60 ml/min) at 450 °C for 12 h and then in vacuum (10^{-3} Pa) for 1 h (fresh sample) and only at 150 °C in vacuum (10^{-3} Pa) for 1 h for the coked samples. The IR spectra were carried out at room temperature after the activation period and after pyridine adsorption at 150 °C and then thermodesorption in vacuum (10^{-3} Pa, 1 h) at increasing temperatures (150, 250, 350, 450, and 500 °C). The concentrations of Brönsted and Lewis acid sites able to retain pyridine at a given temperature were determined using the absorbance surfaces of the corresponding bands at 1545 and 1450 cm^{-1}, respectively, and the extinction coefficients previously determined [29].

The coke content of the samples was measured by total burning at 1020 °C under helium and oxygen with a Thermoquest analyzer. The identification of the coke components was performed using the method previously developed in our laboratory: the zeolite is dissolved in a hydrofluoric acid solution and then the soluble part of the carbonaceous compounds is recovered with methylene chloride and analyzed through GC/MS [30].

2.3. Transformation of *m*-xylene

The transformation of *m*-xylene (Fluka, > 99 wt%) was carried out in a fixed-bed reactor under the following conditions: 350 °C, atmospheric pressure, $P_{m\text{-xylene}}/P_{N_2} = 13$, contact time (taken as the reverse of the weight hourly space velocity) $\tau = 0.0043$ to 0.0694 h/(g_{cat} $g_{hydrocarbon}$). *m*-Xylene was percolated on a silica gel column in order to eliminate traces of peroxide. Before reaction, the catalyst was activated in situ at 450 °C under dry air flow (60 ml/min) overnight and then cooled to the reaction temperature under nitrogen flow. Analysis of reaction products was performed on line by FID gas chromatography using a 60-m fused silica J&W DB Wax capillary column. After reaction, the sample is quickly cooled down to room temperature under nitrogen flow and kept in refrigerator.

3. Results

3.1. Physicochemical characteristics of the MCM-22 zeolite

Scanning electron microscopy shows that the sample is mainly constituted of platelets with a thickness of approximately 0.1 μm and a size of 1 × 1 μm, associated into particles. The nitrogen adsorption isotherm has been analyzed by both the Dubinin–Raduskevitch (DR) and *t*-plot methods using the Harkins–Jura equation [31]. The micropore volume (pore diameter < 20 Å) estimated with both methods, V_{DR} and V_{t1}, respectively, in Table 1, represents approximately 65% of the total pore volume (estimated at $P/P_0 = 0.97$). The difference between total and micropore volumes (35%) is mainly due to interparticular mesopores. The external surface estimated by the *t* plot method was found to be equal to 35 m^2 g^{-1}.

Fig. 1 represents the IR spectra of the sample in the OH-stretching region, before and after pyridine adsorption at 150 °C and desorption at temperatures between 150 and 500 °C. In agreement with previous works [32,33], four hydroxyl bands appear before pyridine adsorption (Fig. 1). The main one at 3620 cm^{-1} (with a shoulder at 3580 cm^{-1}) corresponds to bridged hydroxyl groups. The band at 3660 cm^{-1} is related to hydroxyl groups linked to extraframework Al species (EFAL), probably formed during the calcination procedure. Finally, the bands at 3730 and 3745 cm^{-1} can be attributed to internal and external silanol groups, respectively [32].

Adsorption of pyridine followed by evacuation at 150 °C (Fig. 1) shows that all the bridged hydroxyl groups (band at 3620 cm^{-1} and shoulder at 3580 cm^{-1}) interact with pyridine. These bands reappear after pyridine desorption at 350 °C, their intensity being totally recovered only after desorption at 500 °C. The intensities of the bands at 3660 and 3730 cm^{-1} corresponding to hydroxyl groups of EFAL

species and to internal silanols, respectively, are also significantly decreased. Most likely this is not due to their acidity. For the band at 3660 cm^{-1}, this could be due to the Lewis character of the EFAL species and for the band at 3730 cm^{-1} to interactions between the silanol and the aromatic ring of pyridine adsorbed on bridged hydroxyl groups or on Lewis sites. Furthermore, the band at 3745 cm^{-1}, attributed to external silanol groups, is not affected by pyridine adsorption.

The concentrations of Brönsted and Lewis sites were estimated from the intensities of the bands at 1545 and 1450 cm^{-1} corresponding to pyridinium (Py-H^+) and to pyridine coordinated to Lewis sites (Py-L), respectively, using the extinction coefficients previously determined [29]. The values obtained after pyridine desorption at 150 °C are equal to 632 and 69 μmol g^{-1} for Brönsted and Lewis sites, respectively. Table 1 shows that after desorption at 450 °C pyridine remains adsorbed on most of the Lewis sites but on only 4% of the Brönsted sites, which means that Lewis sites are stronger than Brönsted sites.

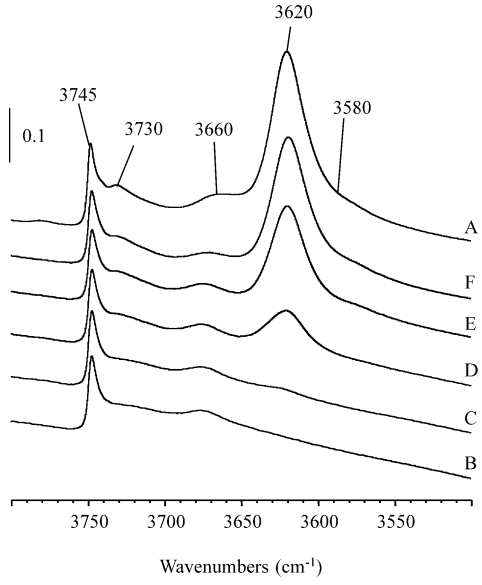

Fig. 1. IR spectra of the fresh MCM-22 sample in the OH-stretching region. (A) Before pyridine adsorption; (B–F) after pyridine evacuation at 150, 250, 350, 450, and 500 °C, respectively.

3.2. *m*-Xylene transformation

As it was previously observed with *n*-heptane cracking at 450 °C [34,35] there is a rapid initial deactivation of *m*-xylene transformation followed by a quasi plateau in activity. Whatever the contact time, the catalyst activity becomes quasi constant for time on stream (TOS) longer than 10 min (Fig. 2). The activities of the fresh and stabilized catalysts were estimated from the slope of the tangent at contact time zero to the curves conversion at TOS = 2 and 60 min vs contact time (Fig. 3A). TOS = 2 min is the lowest value at which the reactant pressure can be considered as constant (even for the lowest contact time values), from the sum of the surface areas of the GC peaks. The activity of the fresh catalyst is equal to 140 mmol h^{-1} g^{-1} and the activity per protonic acid site able to retain pyridine adsorbed as pyridinium ion at 150 °C (i.e., the turnover frequency, TOF) to 220 h^{-1}. The activity of the stabilized catalyst (after 60 min reaction) is equal to 95 mmol h^{-1} g^{-1}.

Whatever contact time and TOS, the products expected from isomerization (*o*- and *p*-xylene) and disproportionation (toluene and trimethylbenzenes) can be observed. However, the molar toluene to TMB ratio is higher than one; furthermore *p*-xylene is strongly favoured with respect to *o*-xylene especially at low conversion. With the fresh catalyst but not on the stabilized sample, other products, C_2–C_4 alkanes and

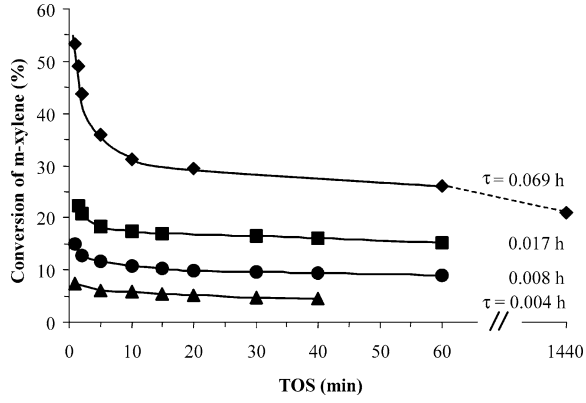

Fig. 2. Conversion of *m*-xylene vs time on stream (TOS). Influence of the contact time τ (taken as the reverse of the weight hourly space velocity).

Table 1
Physicochemical characteristics of the MCM-22 zeolite sample

Pore distribution		Acidity				
		T (°C)	N_B (μmol g^{-1})	A/A_0 B	N_L (μmol g^{-1})	A/A_0 L
V_{total} (cm^3 g^{-1})	0.242	150	632	1	69	1
V_{DR} (cm^3 g^{-1})	0.196	250	584	0.92	62	0.9
V_{t1} (cm^3 g^{-1})	0.202	350	354	0.56	62	0.9
V_{meso} (cm^3 g^{-1})	0.046	450	23	0.04	42	0.61
S_{ext} (m^2 g^{-1})	35.0	500	3	0.005	25	0.36

V_{total}, total pore volume; V_{DR}, micropore volume using the Dubinin–Raduskevitch equation; V_{t1}, micropore volume using the *t*-plot method; V_{meso}, mesopore volume; S_{ext}, external surface using the *t*-plot method; T, pyridine desorption temperature; N_B/N_L, number of Brönsted/Lewis acid sites; A/A_0 B/A/A_0 L, relative number of Brönsted/Lewis acid sites.

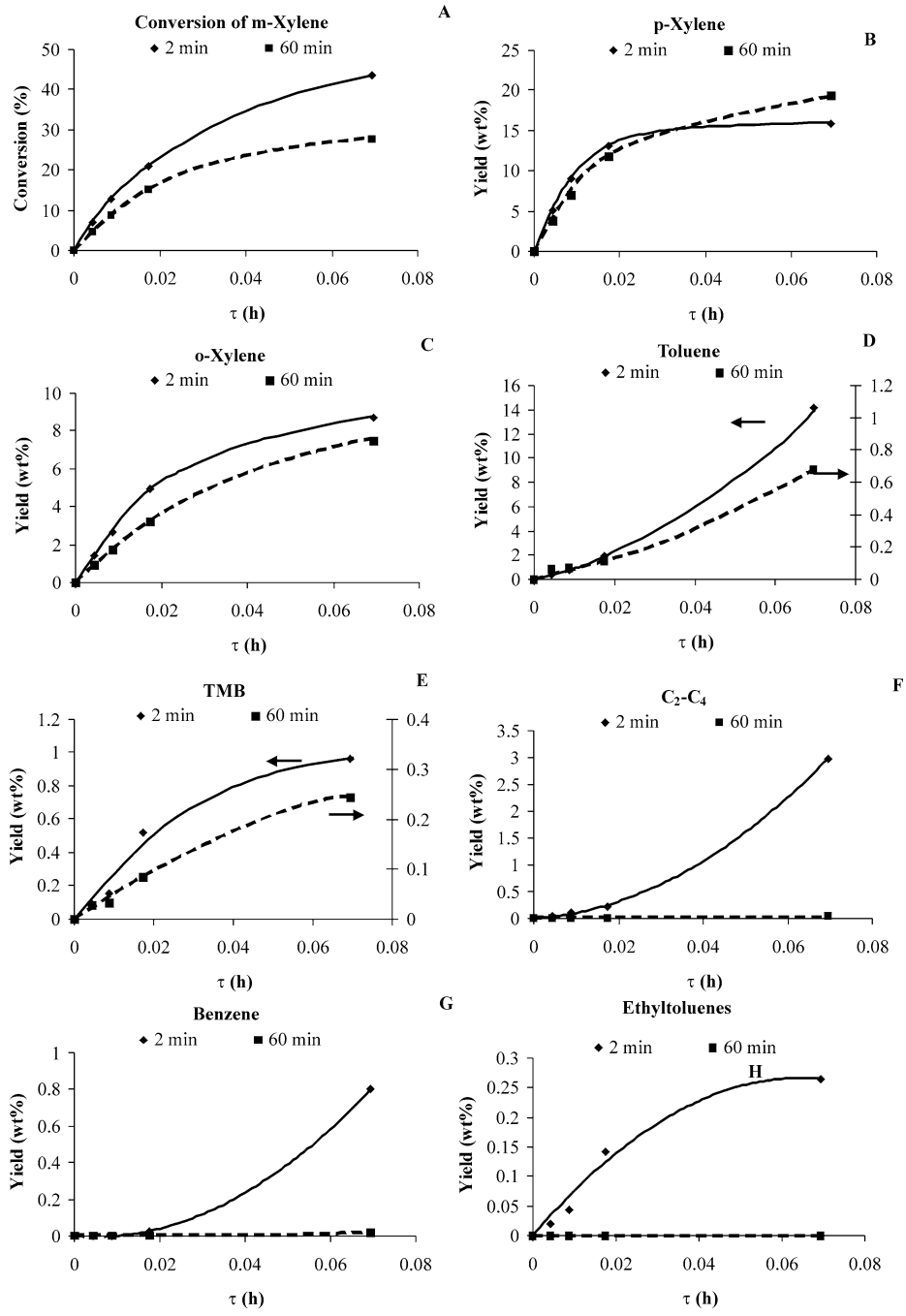

Fig. 3. *m*-Xylene transformation over the fresh (2 min reaction) and stabilized (60 min reaction) MCM-22 sample. Yields in the various products as a function of contact time τ.

alkenes, benzene, and ethyltoluenes can also be observed (Table 2).

Fig. 3 shows that, on the fresh catalyst, xylene isomers, toluene, TMB, and ethyltoluenes, which could result from TMB isomerization, appear as primary products whereas the other products, C_2–C_4 and benzene, result from the transformation of primary products. The shape of the curves giving the yields in *p*- and *o*-xylenes, TMB, and ethyltoluenes vs contact time (Figs. 3B, C, E, and H) is furthermore in agreement with a secondary transformation of these products. A completely different curve is obtained for toluene, with a large increase in toluene yield at long contact times, which indicates a secondary mode of formation of this product. The comparison of the curves in Fig. 3 after 2 and 60 min shows that deactivation has no effect on the direct formation of toluene, practically no effect on *p*-xylene formation (rate divided by 1.3) and a larger effect on *o*-xylene (/1.5) and TMB formation (/2.2); furthermore the formation of C_2–C_4 products, benzene and ethyltoluenes as well as the secondary formation of toluene are completely suppressed.

Table 2
Transformation of *m*-xylene at 350 °C on the fresh (time on stream, TOS = 2 min) and stabilized MCM-22 sample (TOS = 60 min); influence of contact time τ

Time on stream (min):	2				60			
Contact time (h):	0.0043	0.0087	0.0174	0.0694	0.0043	0.0087	0.0174	0.0694
Conversion (%):	7.00	12.75	20.79	43.72	4.76	8.85	15.21	27.75
	Product yields (wt%)							
C_2–C_4	0.05	0.12	0.23	2.98	0.00	0.00	0.00	0.04
Benzene	0.00	0.00	0.02	0.80	0.00	0.00	0.00	0.02
Toluene	0.35	0.74	1.89	14.13	0.06	0.07	0.11	0.68
p-Xylene	5.10	9.02	13.01	15.84	3.71	7.02	11.78	19.26
o-Xylene	1.40	2.66	4.96	8.72	0.95	1.72	3.22	7.49
Et-toluene	0.02	0.04	0.14	0.26	0.00	0.00	0.00	0.00
TMB (% 1,2,4)	0.09 (66.7)	0.15 (78.8)	0.52 (74.0)	0.96 (67.7)	0.03 (51.1)	0.03 (68.4)	0.08 (75.7)	0.24 (70.5)
TeMB	0.02	0.02	0.02	0.03	0.01	0.00	0.01	0.02
	Molar ratios							
p/*o*	3.64	3.39	2.63	1.82	3.90	4.08	3.66	2.57
T/TMB	5.1	6.3	4.8	19.2	2.9	2.7	1.8	3.6

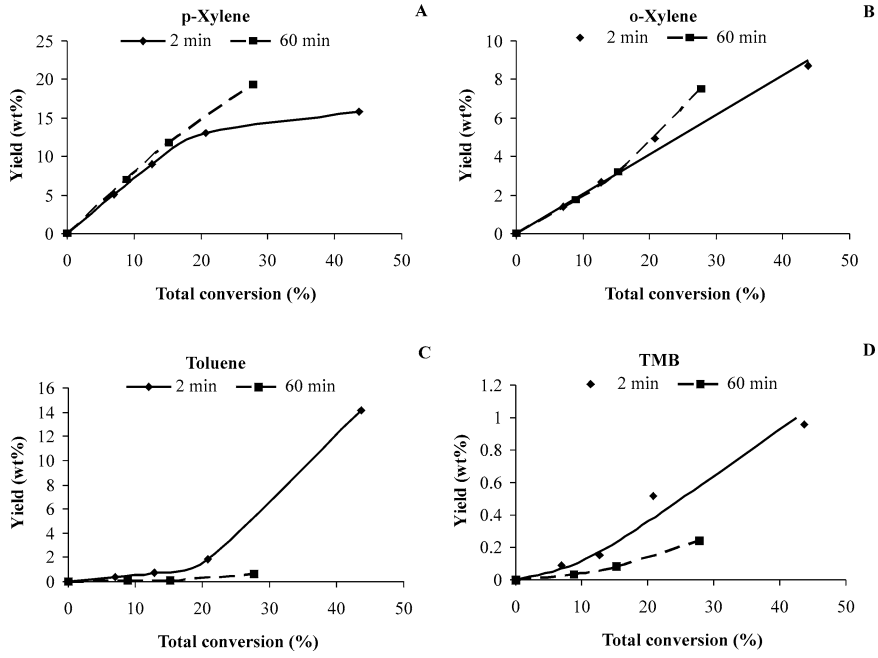

Fig. 4. *m*-Xylene transformation over the fresh (2 min reaction) and stabilized (60 min reaction) MCM-22 sample. Yields in the main products as a function of *m*-xylene conversion.

The yields in the primary products on the fresh and stabilized samples were plotted as a function of *m*-xylene conversion (Fig. 4). At low conversion, deactivation has practically no effect on the selectivity to *ortho* and *para* isomers; at high conversion, the selectivity to isomers is higher on the stabilized than on the fresh sample (Figs. 4A and B). Deactivation causes also a small increase of the *para*/*ortho* ratio. However, the main effect of deactivation deals with the selectivity to toluene and TMB which is significantly decreased (Figs. 4C and D) and to the other products (C_2–C_4 products, benzene, and ethyltoluenes) which no more appear on the stabilized samples.

3.3. Composition of coke and effect on acidity and porosity

For the experiments reported in Table 2, the coke content of the samples was measured at TOS = 60 min and the conversion of *m*-xylene into coke was determined. Fig. 5A shows a quasi-linear increase in conversion for short contact times with an additional coke formation at long contact times. Furthermore, the effect of TOS on coking was determined for the longest contact time (Fig. 5B). Coke is mainly deposited during the first minutes of reaction: thus after 2.5 min reaction the coke content is equal to 2 wt%, after 120 min to 3.5 wt%, and after 24 h to 4.1 wt%. At short TOS, the conversion of *m*-xylene into coke is relatively sig-

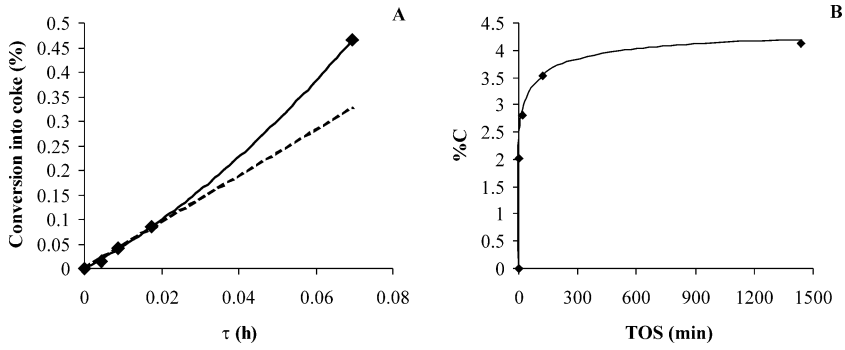

Fig. 5. Formation of coke during *m*-xylene transformation over a MCM-22 sample. (A) Conversion of *m*-xylene into coke as a function of contact time τ; (B) total coke content (% C) as a function of time on stream (TOS) for a contact time τ of 0.069 h.

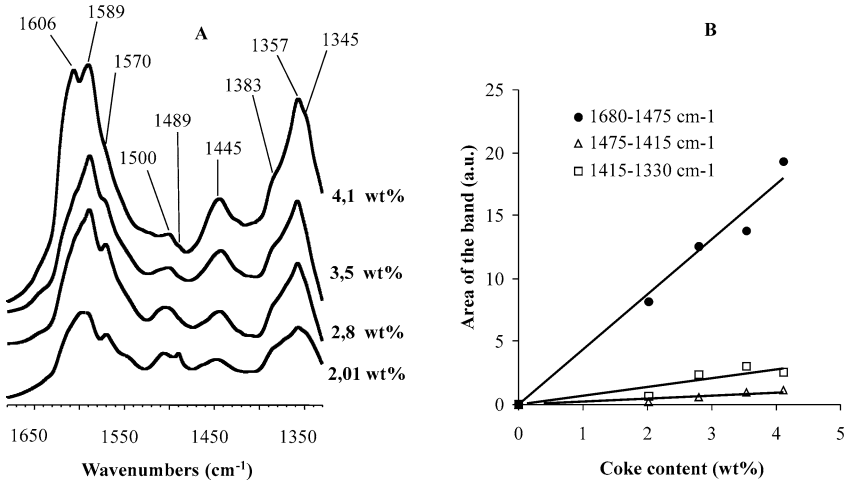

Fig. 6. (A) IR spectra of the coked MCM-22 samples in the 1300–1700 cm^{-1} region. (B) Areas of the bands of coke vs coke content.

nificant: 3.5% during the 2.5 min reaction for a conversion of 42% into desorbed products. Both Figs. 5A and 5B suggest that the carbonaceous deposits (coke) can be considered as primary products.

3.3.1. Composition of coke

The composition of carbonaceous deposits (coke) was determined for the four samples used in the experiments of Fig. 5B. With all these samples, all the carbonaceous compounds were found to be soluble in methylene chloride after dissolution of the zeolite in hydrofluoric acid. Furthermore, no carbonaceous compounds were recovered in methylene chloride after a simple soxhlet treatment (without acid treatment), which shows that all the "coke" components are trapped inside the pores.

Analysis of coke by GC-MS shows that coke consists of six different families of components, all being methyl-substituted aromatic hydrocarbons:

- Trimethyl and tetramethylbenzenes: family A;
- Methylnaphtalenes (1–4 methyl groups): family B;
- Methylphenanthrenes (1–5 methyl groups): family C;
- Methylpyrenes (1–6 methyl groups): family D;
- Methyldibenzofluorenes (2–5 methyl groups): family E; and
- Methyldibenzofluoranthenes (2–6 methyl groups): family F.

The chemical nature (methyl aromatic compounds) of coke components was confirmed by IR spectroscopy of the coked samples (see for instance in Fig. 6A the bands in the 1300–1700 cm^{-1} region). As was shown by other authors [36,37] the integrated absorbances of the bands are proportional to the amount of coke deposited on the zeolite (Fig. 6B).

The quantitative distribution of coke molecules estimated by GC is given in Fig. 7 as a function of coke content. At low coke contents (2.0 or 2.8 wt%), hence at short TOS, coke is mainly composed of families A, B, and C whereas at high coke contents (e.g., 4.1 wt%) hence at long TOS only families D, E, F are present. From Fig. 7 and from the chemical nature of the coke components, the following scheme can be proposed for coke formation (Scheme 1).

3.3.2. Influence of coke on porosity and acidity

Fig. 8 shows that coke does not affect the access of nitrogen to the mesopore volume but causes a significant decrease

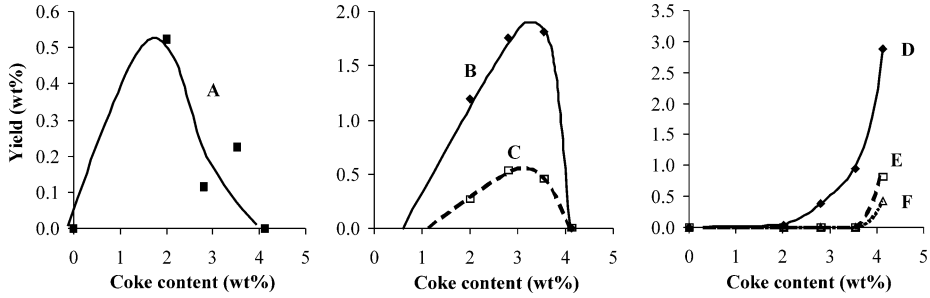

Fig. 7. Yields in the coke components as a function of coke content. (A) Tri and tetramethylbenzenes, (B) methylnaphtalenes, (C) methylphenanthrenes, (D) methylpyrenes, (E) dibenzofluorenes, (F) dibenzofluoranthenes.

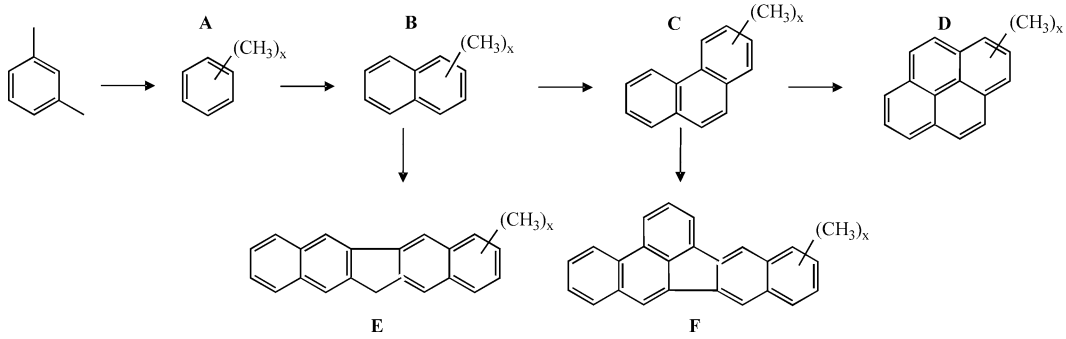

Scheme 1.

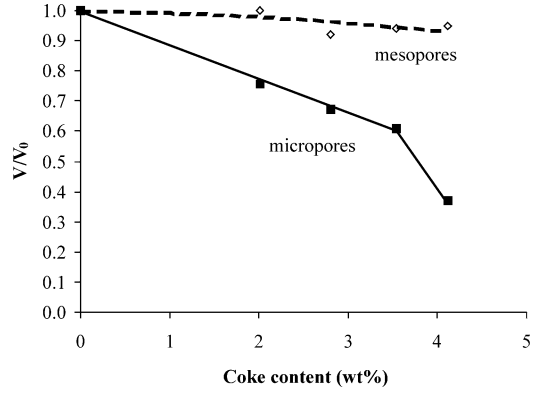

Fig. 8. Residual micropore and mesopore volumes accessible to nitrogen vs coke content.

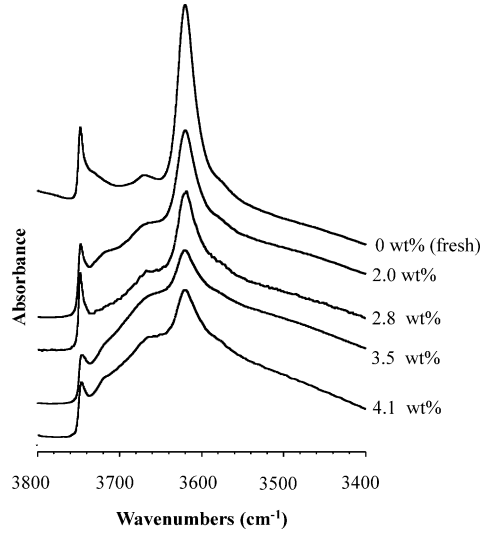

Fig. 9. IR spectra of fresh and coked MCM-22 samples in the OH-stretching region.

in the access to the micropore volume. Up to 3.5 wt% coke, this decrease is proportional to the coke content; above this value the effect of coke becomes more significant.

Coke has a large decreasing effect on the intensity of the bridging OH band and causes also the formation of a very large band between 3500 and 3650 cm^{-1}, most likely due to interaction between carbonaceous compounds and silanol groups (Fig. 9). Whatever the coke content, all the bridging OH groups interact with pyridine molecules at 150 °C. A semiquantitative estimation of the effect of coke on the bridging OH groups was made on the spectra obtained by difference between spectra after activation and after pyridine adsorption–desorption at 150 °C. Up to 3.5 wt%, a linear decrease in the intensity of the bridging OH band can be observed. Above this value (from 3.5 to 4.1 wt%), the intensity of the band remains constant (Fig. 10).

The concentrations of Brönsted and Lewis sites on the coked samples were determined from the intensity after desorption at 150 °C of the bands corresponding to pyridinium ions (1545 cm^{-1}) and to pyridine coordinated to Lewis acid sites (1450 cm^{-1}) by using the extinction coefficients previously determined [29]. Curiously, the effect of coke is much weaker on the concentration of protonic sites interacting with pyridine than on the intensity of the bridging OH band.

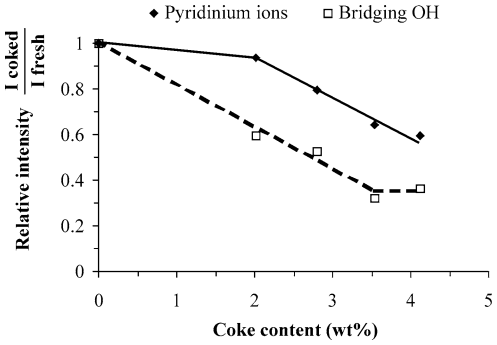

Fig. 10. Effect of coke on the relative intensities of the bridging OH band and of the pyridinium band on the coked and fresh MCM-22 samples.

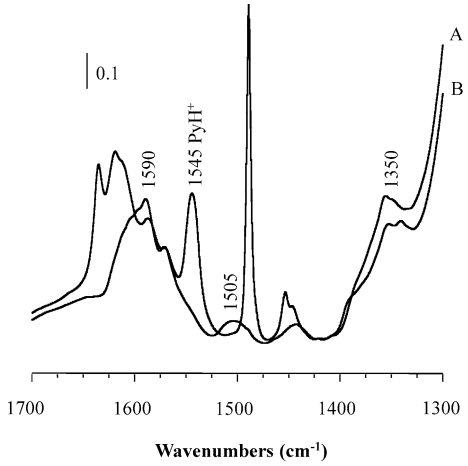

Fig. 11. IR spectra of the 20 min coked MCM-22 sample before (A) and after (B) pyridine adsorption.

The difference is particularly pronounced at low coke contents, the first deposits of coke (2 wt%) having practically no effect on the concentration of protonic sites determined by pyridine adsorption. Similar observations were previously made [38] and explained by a displacement of coke molecules from the protonic sites on which they were adsorbed. To confirm this proposal, the intensities of the IR bands corresponding to coke molecules were compared before and after pyridine adsorption. With all the coked samples (see, as an example, the sample coked for 20 min TOS in Fig. 11), a significant decrease of the bands at 1350, 1505, and 1590–1600 cm^{-1}, which do not overlap on the bands of pyridine, can be observed.

Furthermore, only small and nonsystematic changes with coke content in the concentration of Lewis sites retaining pyridine adsorbed can be observed (69, 76, and 63 $\mu mol\, g^{-1}$ for coke contents of 0, 2.0, and 4.1 wt%, respectively). This observation, already made by various authors [38,39] could indicate that Lewis acid sites are inactive in coke formation.

4. Discussion

On the fresh HMWW zeolite, a large variety of products are formed through the primary reactions generally observed, i.e., isomerization and disproportionation, but also through secondary transformations of the primary products. During the first moments of reaction, a significant decrease in activity and a very large change in product distribution were found. These observations can be related to the formation inside the zeolite pores of carbonaceous compounds (coke) which cause a decrease in the accessibility of organic molecules to part of the acidic acid sites.

Proposals will be made to explain the mode of formation of desorbed products and coke. The location in the different pore systems of the MCM-22 zeolite of coke molecules as well as of the acid sites active in the formation of the various products will be specified.

4.1. Reaction scheme

The scheme reported in Fig. 12 can be proposed for *m*-xylene transformation on the fresh H-MWW samples.

Isomers and disproportionation products are directly formed (primary products). Isomerization (reaction 1, Fig. 12) is approximatively 10 times more faster than disproportionation (reaction 2, Fig. 12). The *para* to *ortho*-xylene ratio is high (close to 4 at low conversion), which indicates shape-selectivity effects. This suggests that a large part of isomerization occurs in the supercages or in the sinusoidal channels with significant limitations in the desorption of the bulkier *ortho* isomer through the narrow apertures of these pores. Indeed, limitations in *o*-xylene desorption from the large pockets of the external surface (7.1 Å ∅, 9 Å) are most unlikely.

On the other hand, the toluene to trimethylbenzenes ratio is much higher than one (Table 2). That can be explained by strong limitations in the desorption of TMB from the internal micropores. Part of the TMB are furthermore found in coke (family A), which means that they are quasi-irreversibly retained in these micropores. Because of their long residence time in the micropores, the transformation of TMB into desorbed and nondesorbed products is most likely. Xylene disproportionation being a bimolecular reaction involving bulky trimethyldiphenylmethane intermediates is probably limited by steric constraints in the sinusoidal channels, and hence should occur preferably in supercages (7.1 Å ∅, 18.4 Å). However, molecular modeling shows that disproportionation of *m*-xylene could occur within the sinusoidal channels (interaction energy with trimethyldiphenylmethane intermediates of $-140\ kcal\, mol^{-1}$) (S. Laforge, unpublished results).

Ethyltoluenes appear as primary products (Fig. 3H). These compounds result most likely from isomerization of TMB inside the micropores; they appear as primary products because TMB desorption is strongly limited compared to isomerization and especially desorption of the slim eth-

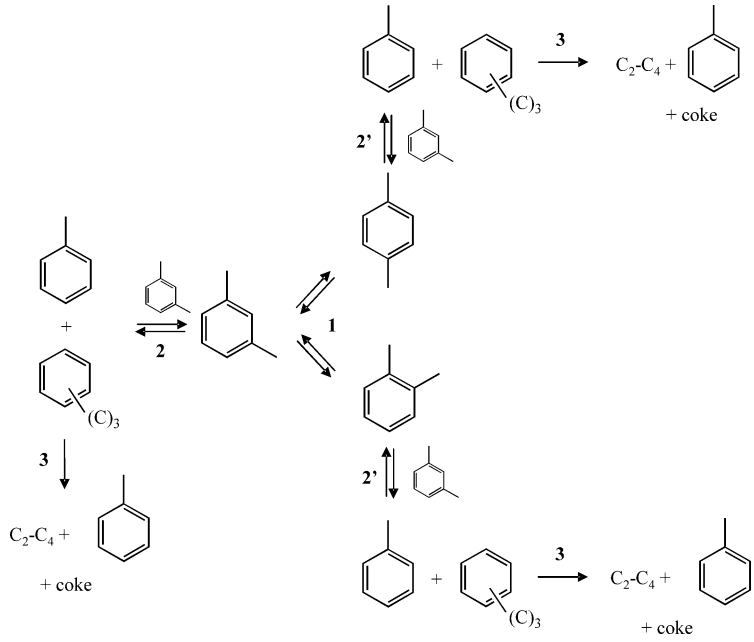

Fig. 12. Scheme of *m*-xylene transformation over the fresh MCM-22 sample. 1, isomerization; 2, disproportionation; 2′, transalkylation; 3, secondary transformation of trimethylbenzenes.

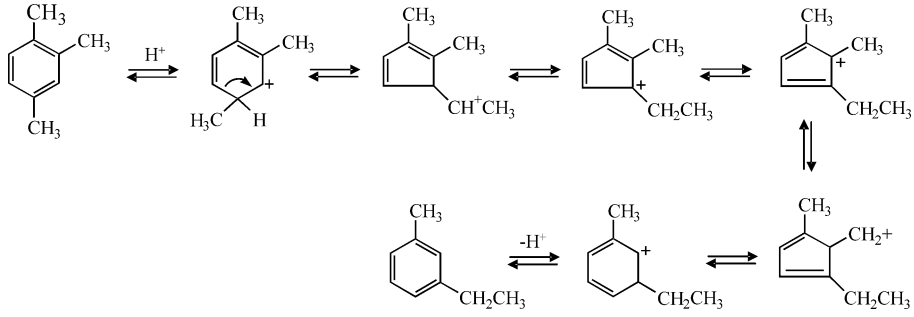

Fig. 13. Mechanism of trimethylbenzene isomerization into ethyltoluene.

yltoluene molecules. Acid isomerization of TMB into ethyltoluenes is, however, a relatively difficult reaction with 6,5-ring contraction and 5,6-ring expansion steps (Fig. 13). This type of reaction was shown to play a significant role in methanol transformation into short-chain alkenes because of long contact times of polymethylbenzene molecules inside the micropores of zeolites (MFI, MOR, and BEA) or of SAPO-34 [40]. It explains also the formation of isobutane by hydrocracking of hexamethylbenzene (paring reaction [41]).

Like ethyltoluenes, C_2–C_4 products and coke result most likely from secondary transformations of TMB in the internal micropores (reaction 3, Fig. 12). In these micropores, TMB molecules can undergo various reactions:

(a) Transformation into tetramethylbenzenes (which are A coke components) through disproportionation or transalkylation with xylenes or toluene. Penta and hexamethylbenzenes could also be formed through the same reactions. The desorption of these bulky molecules through the small apertures of the supercages (4.0×5.5 Å) is most unlikely.

(b) Isomerization of the tri- and tetra-methylbenzenes into ethylmethylbenzenes through the mechanism described in Fig. 13. 6,5-Ring contraction and 5,6-ring expansion involved in this mechanism could also allow the formation of propyl(methyl)benzene molecules.

(c) Dealkylation of ethylmethylbenzene molecules and (if they can be formed) of propylmethylbenzene molecules.

(d) Transformation of ethylene and eventually propene through oligomerization and cracking reactions into C_2–C_4 olefinic compounds.

(e) Transformation of the tri- and tetra-methylbenzene molecules (A coke components) into the other families of coke components according to Scheme 1.

The results reported in Table 2 for TOS = 2 min are in good agreement with these reactions. Indeed toluene and TMB are found to be formed in quasi-equimolar amounts by disproportionation when C_2–C_4 products, coke, and part

of toluene are considered to result from secondary transformations of TMB.

Benzene is also observed in the reaction products but only at the longest contact time on the fresh zeolite. Most likely this product results from transalkylation between *m*-xylene and toluene which is formed in large amounts under these conditions.

Xylene isomers can also undergo secondary transformations. This is clearly shown for *p*-xylene by the quasi plateau observed at long contact time for the yield in this product (Fig. 3B) although this yield is relatively far from thermodynamic equilibrium. A decrease in the rate of *o*-xylene production can also be observed at long contact time, suggesting secondary transformations of this isomer (Fig. 3C). Most likely these isomers react with *m*-xylene leading to TMB and toluene by transalkylation (reaction 2′, Fig. 12), a large part of TMB being afterward transformed into secondary products. This explains the secondary formation of C_2–C_4 hydrocarbons (Fig. 3F), toluene (Fig. 3D), and coke (Fig. 5A) which is observed at long contact times.

The effect of deactivation depends very much on the product and on the contact time. Thus, at short contact times, the rates of formation of the main primary products, *p*-xylene, *o*-xylene, toluene, and TMB are divided by 1.35, 1.5, 6.0, and 3.0, respectively. At long contact times, the rate of *p*-xylene formation is greater on the stabilized than on the fresh catalysts (Fig. 3B) and for *o*-xylene the effect of deactivation becomes lower (Fig. 3C). For toluene (Fig. 3D), deactivation suppresses the secondary mode of formation. For TMB (Fig. 3E), the effect of deactivation is quasi similar at short and long contact times. However, the main effect of deactivation is to completely suppress the formation of C_2–C_4, benzene, ethyltoluenes (Figs. 3F–H) and coke (Fig. 5B). All these products result from secondary transformations of TMB, which means that deactivation decreases very significantly the primary formation of TMB by xylene disproportionation. This decrease is probably responsible for the unexpected increase with deactivation of *p*-xylene formation which was observed at long contact times (Fig. 3C). On the stabilized catalyst, all the *p*-xylene resulting from isomerization appears in the reaction products whereas on the fresh catalyst, part of *p*-xylene would be transformed via TMB into C_2–C_4 hydrocarbons, toluene, and coke. The decrease observed at long contact times in the effect of deactivation on *o*-xylene formation can be explained by the same way.

4.2. Mechanism of coke formation

During transformation of aromatic reactants over acid catalysts, coke can be formed through different modes [42]. The most common involves the formation of transalkylation intermediates followed by creation of an additional cycle either aromatic or fluorenic. Thus, the pentamethyldiphenylmethane compounds which are intermediates in TMB disproportionation can undergo (i) cyclization and hydrogen transfer steps leading to tetramethylanthracenes (Scheme 2), hence with creation of two additional aromatic rings (Scheme 2), or (ii) dihydrogenating coupling plus hydrogen transfer leading to pentamethylfluorenes (Scheme 3).

Scheme 3 is most likely responsible for the formation of E and F coke molecules from B and C molecules (Scheme 1) but does not seem to play a role in the growth of coke molecules. Indeed, the transformation of A into D coke molecules is clearly successive with the formation of only one (and not two) aromatic ring by step.

This growth of coke molecules by creation of only one aromatic ring occurs only in presence of olefinic com-

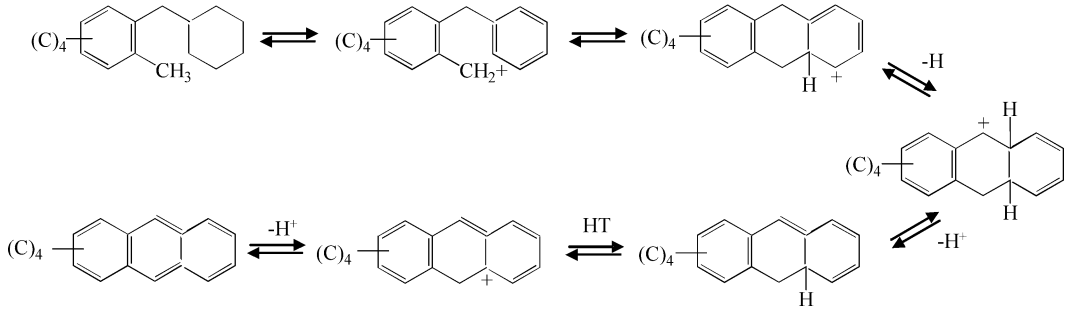

Scheme 2.

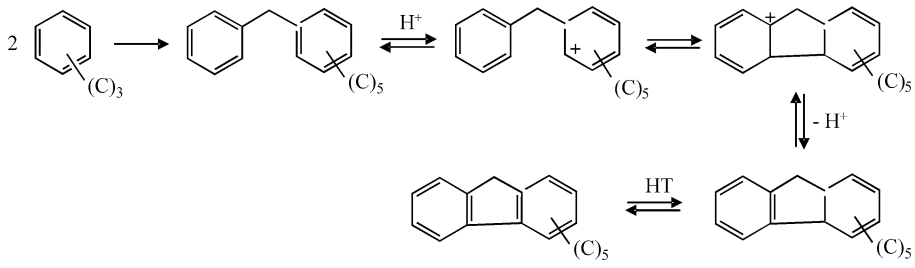

Scheme 3.

pounds [42]. This creation involves a series of alkylation, cyclization, isomerization, and hydrogen transfer steps. Olefinic compounds are involved not only in aromatic alkylation but also in hydrogen transfer steps in which they are transformed into alkanes.

4.3. Location of coking and of the other reactions

Coke molecules are necessarily located in the internal micropores, either in the supercages or in the sinusoidal channels. Indeed, although all the coke molecules were found to be soluble in methylene chloride, none of them could be recovered by the direct soxhlet treatment of the coked samples and hence could be located in the hemicages of the outer surface.

It is most likely that the formation of coke molecules which involves bimolecular transformations, alkylation, hydrogen transfer, disproportionation and hence bulky intermediates occurs preferentially in the large cylindrical supercages (7.1 Å ∅, 18.4 Å) and not at the intersection of sinusoidal channels (5.8 Å) or in the small cages located along these channels (6.9 × 6.4 Å) [32]. Furthermore, it is well known that coking is highly favored when the zeolites present trap cages (large cages with small apertures) [43]. Moreover, in a previous study dealing with coke formation during *n*-heptane cracking at 450 °C [34,35], it has been demonstrated experimentally and by molecular modeling that highly polyaromatic molecules could be formed and trapped in the supercages whereas only naphtalene molecules without a methyl group were formed and retained in the small cages along the sinusoidal channels.

Fig. 7 shows that families C, D, E, and F, which are constituted of coke molecules too bulky to be accommodated in the sinusoidal channels, result from total transformation of methylnaphtalene molecules (family B). This proves that methylnaphtalenes (family B), TMB, and tetramethylbenzenes (family A) are formed in the supercages and not in the sinusoidal channels.

Therefore, the deposit of coke should only affect the reactions which occur in the supercages. When all the protonic sites of the supercages are either poisoned or made inaccessible to the reactant molecules by carbonaceous deposits, only the products formed on the protonic sites located in the sinusoidal channels system and in the pockets of the outer surface will be formed. This situation seems to occur after 120 min of reaction. Indeed at this time, 70% of the protonic bridging hydroxyls, which corresponds approximately to the percentage of sites present in the supercages [32], interact with coke molecules (Fig. 10). At TOS ⩾ 120 min, *m*-xylene is mainly transformed through isomerization, the *para* isomer being largely favored: *para*/*ortho* ratio of 3.6 at 20% conversion, which corresponds to approximately 5 at zero conversion. This high value of the *para*/*ortho* ratio suggests that a large part of isomerization occurs in the narrow sinusoidal channels from which *o*-xylene desorption is strongly limited. However isomerization in the outer pockets which led most likely to quasi-equivalent amounts of the *ortho* and *para* isomers cannot be excluded. Disproportionation can also be observed on the stabilized catalyst hence in the sinusoidal channels or in the outer pockets or in both. However this reaction is practically negligible in comparison to isomerization: disproportionation/isomerization ratio close to 0.01.

For both reactions, no deactivation can be observed, which can be related to the very low rate of coke formation in the sinusoidal channels and in the external pockets. Within the narrow sinusoidal channels, the low coking rate is mainly due to the steric inhibition of the bimolecular reactions which are required for the formation of bulky secondary products. In addition, most of the molecules which can be formed can desorb from the sinusoidal channels because of the quasi-identical sizes of the channel apertures and the channel intersections. On the other hand, the absence of coking in the external cups can be related to the fact that disproportionation of aromatics which is an essential step in coke formation is very unfavored in the external cups of MCM-22 zeolite [16,44]. However, we suggest that the main reason is that coke formation, besides reaction steps, requires the coke precursors to be retained long enough to be transformed into larger molecules, irreversibly blocked in the pores [43], which seems very difficult in large external cups with small depth.

The reactions occurring in the supercages are those which disappear with deactivation. The participation of the protonic sites of the supercages in the transformations of *m*-xylene was estimated at low conversion, i.e., at short contact times (columns 1 and 5 of Table 2). Approximately 30% of *p*-xylene and *o*-xylene disappear by deactivation; hence 30% of isomerization would occur in the supercages. A *para*/*ortho* ratio of 3 was found for this reaction, indicating limitations in the desorption of *o*-xylene through the narrow apertures (4.0 × 5.5 Å) of the supercages. All the other products result from disproportionation (toluene, TMB) or from secondary transformation of TMB (ethyltoluenes, C_2–C_4, and coke). By considering all these products as resulting from disproportionation it was found that approximately 85% of this reaction occurred in the supercages. As it is expected in large cages, the isomerization to disproportionation ratio is relatively high (0.25). Furthermore, as it was previously indicated, the secondary transformations of TMB occur totally in the supercages.

5. Conclusions

On a MCM-22 zeolite at 350 °C, *m*-xylene transforms directly through isomerization and disproportionation. The *para* isomer is largely favored compared to the *ortho* isomer, which indicates limitations in the desorption of this latter isomer. The molar toluene to trimethylbenzene ratio is much higher than one showing that part of TMB undergoes secondary transformations before desorbing from

the zeolite. The following secondary reactions were shown to occur: transalkylation TMB–*m*-xylene with formation of toluene and of tetramethylbenzenes which remain trapped in the zeolite micropores, isomerization of TMB (and tetramethylbenzenes) into ethyl aromatic compounds, dealkylation of ethyl aromatics, oligomerization-cracking of ethylene, and transformation of the TMB, tetramethylbenzenes, and light olefins into carbonaceous compounds (coke) responsible for catalyst deactivation.

Coke was shown to consist of six families of components with one to five aromatic rings bearing methyl groups. The scheme of coking and the main reactions involved in coke formation were established. From this scheme and from the comparison between the size of coke molecules and of the micropores, it was concluded that coking occurs in the supercages only.

On the stabilized catalysts, all the bridging OH groups of the supercages of the MCM-22 zeolite were shown by IR spectroscopy to interact with coke molecules. Therefore, the reactions observed on the stabilized MCM-22 zeolite, essentially isomerization with a highly favored formation of the *para* isomer, are those catalyzed by the protonic sites of the sinusoidal channels and of the pockets located on the outer surface; practically no coke formation and hence no decrease in activity can be observed.

Furthermore, the reactions which disappear by deactivation, i.e., isomerization of *m*-xylene with a favored formation of the *para* isomer, disproportionation into toluene and trimethylbenzenes, and the secondary transformations of TMB all occur in the supercages. Deactivation is fast due to a rapid formation of secondary products in these trap cages (large cages with small apertures). Whereas the high selectivity to the *para* isomer of *m*-xylene isomerization is in favor of a reaction within the sinusoidal channels it cannot be excluded that part of isomerization occurs in the outer pockets. In the following paper of this series, poisoning experiments were carried out to confirm the location of the various reactions in the three pore systems and especially to specify the role of the protonic acid sites located in the outer pockets.

References

[1] M.K. Rubin, P. Chen, US patent 4,954,325, 1990.
[2] M.E. Leonowicz, S.L. Lawton, R.D. Partridge, P. Chen, M.K. Rubin, Science 264 (1994) 1910.
[3] R. Millini, G. Perego, W.O. Parker Jr., G. Bellussi, L. Carluccio, Micropor. Mater. 4 (1995) 221.
[4] S.L. Lawton, M.E. Leonowicz, R.D. Partridge, P. Chen, M.K. Rubin, Micropor. Mesopor. Mater. 23 (1998) 109.
[5] Ch. Baerlocher, W.M. Meier, D.H. Olson, Atlas of Zeolite Framework Types, 5th ed., Elsevier, Amsterdam, 2001.
[6] A. Corma, C. Corell, A. Martinez, J. Perez-Pariente, in: J. Weitkamp, H.G. Karge, H. Pfiefer, W. Hölderich (Eds.), Zeolites and Related Microporous Materials: State of the Art 1994, in: Stud. Surf. Sci. Catal., Vol. 84, Elsevier, Amsterdam, 1994, p. 859.
[7] A. Corma, C. Corell, F. Llopis, A. Martinez, J. Perez-Pariente, Appl. Catal. A 115 (1994) 121.
[8] A. Corma, A. Martinez, C. Martinez, Catal. Lett. 28 (1994) 187.
[9] A. Corma, V. Gonzàlez-Alfaro, A.V. Orchillès, Appl. Catal. A 129 (1995) 203.
[10] A. Corma, J. Martinez-Triguero, J. Catal. 165 (1997) 102.
[11] S. Unverricht, M. Hunger, S. Ernst, H.G. Karge, J. Weitkamp, in: J. Weitkamp, H.G. Karge, H. Pfiefer, W. Hölderich (Eds.), Zeolites and Related Microporous Materials: State of the Art 1994, in: Stud. Surf. Sci. Catal., Vol. 84, Elsevier, Amsterdam, 1994, p. 37.
[12] H.G. Karge, S. Ernst, M. Weihe, U. Weiß, J. Weitkamp, in: J. Weitkamp, H.G. Karge, H. Pfiefer, W. Hölderich (Eds.), Zeolites and Related Microporous Materials: State of the Art 1994, in: Stud. Surf. Sci. Catal., Vol. 84, Elsevier, Amsterdam, 1994, p. 1805.
[13] W. Souverijns, W. Verrelst, G. Vanbutsele, J.A. Martens, P.A. Jacobs, J. Chem. Soc., Chem. Commun. (1994) 1671.
[14] P. Meriaudeau, Vu A. Tuan, Vu T. Nghiem, F. Lefebvre, Vu T. Ha, J. Catal. 185 (1999) 378.
[15] P. Wu, T. Komatsu, T. Yashima, Micropor. Mesopor. Mater. 22 (1998) 343.
[16] S.-H. Park, H.-K. Rhee, Catal. Today 63 (2000) 267.
[17] A. Corma, V. Martinez-Soria, E. Schnoeveld, J. Catal. 192 (2000) 163.
[18] J.S. Beck, A.B. Dandekar, T.F. Degnan, in: M. Guisnet, J.P. Gilson (Eds.), Zeolites for Cleaner Technologies, in: Catalytic Science Series, Vol. 3, Imperial College Press, London, 2002, p. 223.
[19] T.F. Degnan Jr., C. Morris Smith, C.R. Venkat, Appl. Catal. A 221 (2001) 283.
[20] Hydrocarbon Processing (October 1996) 40.
[21] J.N. Miale, N.Y. Chen, P.B. Weisz, J. Catal. 6 (1966) 278.
[22] H.A. Benesi, B.H.C. Winquist, Adv. Catal. 27 (1978) 97.
[23] M. Guisnet, in: B. Imelik, C. Naccache, G. Coudurier, Y. Ben Taarit, J.C. Vedrine (Eds.), Catalysis by Acids and Bases, in: Stud. Surf. Sci. Catal., Vol. 20, Elsevier, Amsterdam, 1985, p. 283.
[24] P.A. Jacobs, J.A. Martens, New developments in zeolite science and technology, in: Y. Murakami, A. Iijima, J.W. Ward (Eds.), Proceedings of the 7th International Zeolite Conference, Elsevier, Amsterdam, 1986, p. 23.
[25] J. Weitkamp, S. Ernst, R. Kumar, Appl. Catal. 27 (1986) 207.
[26] P.A. Jacobs, J.A. Martens, in: H. van Bekkum, E.M. Flanigen, J.C. Jansen (Eds.), Introduction to Zeolite Science and Practice, in: Stud. Surf. Sci. Catal., Vol. 58, Elsevier, Amsterdam, 1991, p. 445.
[27] N.S. Gnep, J. Tejada, M. Guisnet, Bull. Soc. Chim. Fr. 1–2 (5) (1982).
[28] J.A. Martens, J. Perez-Pariente, E. Sastre, A. Corma, P.A. Jacobs, Appl. Catal. 45 (1988) 85.
[29] M. Guisnet, P. Ayrault, J. Datka, Polish J. Chem. 71 (1997) 1455.
[30] M. Guisnet, P. Magnoux, Appl. Catal. 54 (1989) 1.
[31] W.D. Harkins, G. Jura, J. Chem. Phys. 11 (1943) 431.
[32] D. Meloni, S. Laforge, D. Martin, M. Guisnet, E. Rombi, V. Solinas, Appl. Catal. A 215 (2001) 55.
[33] A. Corma, C. Corell, V. Fornés, W. Kolodziejski, J. Perez-Pariente, Zeolites 15 (1995) 576.
[34] E. Besset, D. Meloni, D. Martin, M. Guisnet, L. Schreyeck, in: B. Delmon, G.F. Froment (Eds.), Catalyst Deactivation 1999, in: Stud. Surf. Sci. Catal., Vol. 126, Elsevier, Amsterdam, 1999, p. 171.
[35] D. Meloni, D. Martin, M. Guisnet, Appl. Catal. A 215 (2001) 67.
[36] H.G. Karge, in: H. van Bekkum, E.M. Flanigen, J.C. Jansen (Eds.), Introduction to Zeolite Science and Practice, in: Stud. Surf. Sci. Catal., Vol. 58, Elsevier, Amsterdam, 1991, p. 531.
[37] H.S. Cerqueira, P. Ayrault, J. Datka, P. Magnoux, M. Guisnet, J. Catal. 196 (2000) 149.
[38] H.S. Cerqueira, P. Ayrault, J. Datka, M. Guisnet, Micropor. Mesopor. Mater. 38 (2000) 197.
[39] A.K. Ghosh, R.A. Kydd, J. Catal. 100 (1986) 188.
[40] M. Guisnet, J. Mol. Catal. A 182–183 (2002) 367.
[41] R.F. Sullivan, C.J. Egan, G.E. Langlois, R.P. Sieg, J. Am. Chem. Soc. 83 (1961) 1156.
[42] M. Guisnet, P. Magnoux, Appl. Catal. A 212 (2001) 83.
[43] M. Guisnet, P. Magnoux, Catal. Today 36 (1997) 477.
[44] R. Gläser, M. Hunger, S. Ernst, J. Weitkamp, Catal. Lett. 50 (1998) 141.